Dramatic improvement of NO reduction activity via reversible re-dispersion of CeO$_2$ nanoparticles into Ce^{+3} atoms on alumina under high temperature reactive treatment

Konstantin Khivantsev,[a]*† Hien Pham[b]†, Mark H. Engelhard[a]†, Xiaohong Shari Li[a], Jinshu Tian[a], Xinyi Wei[c], Yipeng Sun[c], Pascaline Tran[c], Trent R. Graham[a], Dong Jiang[d], János Szanyi[a]*, Abhaya Datye[b]* and Yong Wang[a,d]*

[a]   Dr. Konstantin Khivantsev, Dr. Mark H. Engelhard, Dr. Shari Li, Dr. Jinshu Tian, Dr. Trent Graham, Dr. Janos Szanyi, Dr. Yong Wang
Pacific Northwest National Laboratory
Richland, WA 99352 USA
Emails (correspondence to): Konstantin.Khivantsev@pnnl.gov, Datye@unm.edu, Yong.Wang@pnnl.gov, † denotes equal contribution

[b]   Professor Hien Pham, Professor Abhaya Datye, Chemical & Biological Engineering, University of New Mexico, Albuquerque, NM 87131 USA

[c]   Dr. Xinyi Wei, Dr. Yipeng Sun, Dr. Pascaline Tran, BASF Corporation, Environmental Catalysis, Iselin, NJ, USA

[d]   Dr. Dong Jiang, Professor Yong Wang, Voiland School of Chemical Engineering and Bioengineering, Washington State University
Pullman, WA 99164 USA

Abstract: Ceria nanoparticles supported on gamma-alumina prepared via wet impregnation and sourced commercially have low activity for industrially relevant NO reduction by CO in the presence of steam. These supports contain ceria nanoparticles as well as small (~1%) amount of Ce atomically dispersed and anchored by penta-Al sites. We discovered that treatment of these catalysts at temperatures ~750-950 ºC under the flow of CO and NO in the presence of steam, which typically leads to catalyst deterioration and sintering, in fact, leads to dispersion of ceria nanoparticles into isolated Ce+3 atoms. We extensively characterize them with XPS, FTIR and HAADF-STEM imaging. Their presence changes the alumina surface, as evidenced by XPS and FTIR with probe molecules. Ce+3 ions show dramatically enhanced NO reduction ability in the presence of CO and steam. Infra-red studies reveal close interaction of NO molecules on Ce+3/Alumina surfaces with the formation of N$_2$O species. Heating these samples in oxygen (in wet or dry streams) at 800 ºC and above leads to coalescence of Ce+3 into CeO$_2$ nanoparticles, resulting in reversible loss of activity. Further, reactive treatment of CeO$_2$/Al$_2$O$_3$ under high temperature reaction conditions restores Ce+3 cations as well as catalytic activity. Our study shows reversible redispersion of ceria into isolated Ce+3 cations under conditions where typical catalyst sintering is generally assumed to occur and suggests a pathway to utilize these materials as supports for more effective catalysis. Indeed, supporting only 0.1-0.5 wt% Rh on these CeAl supports, shows synergies between Rh and atomically dispersed Ce ions with excellent activity and stability for NO reduction with CO.

Ceria nanoparticles alone or on supports have emerged as versatile catalysts for various catalytic reactions, such as CO and hydrocarbon oxidation, NO reduction, water-gas-shift, among others [1-35]. Commercial use of ceria commenced ~40 years ago for three-way-catalysts in gasoline engines that are critical to remove NO and CO pollutants. In those applications, ceria is often supported on alumina: without alumina, ceria does not have enough thermal stability and sinters significantly at high temperatures in the presence of steam [3-11]. The ability of ceria to participate in catalysis is often related to its ability to cycle between Ce+4/Ce+3 oxidation states, the mobility of lattice oxygen which can be removed or restored under redox treatments [5-11]. It is generally suggested that maintaining of structural integrity of ceria nanoparticles is key in achieving high catalytic activity [1-30]. Despite great success in understanding ceria materials in automotive applications, there remain unanswered questions that need to be addressed to gain molecular level insight into catalytic behaviour and further potential improvement of these materials: 1). how they perform under real-world exhaust conditions, i.e., in the presence of steam and reactants at high temperatures [3, 6, 35] 2). can ceria avoid sintering under these conditions? 3). What changes occur under red-ox treatments in the presence of steam at elevated temperatures and how they are related to catalysis? Although a wealth of knowledge has been accumulated over decades on the structural behaviour of ceria/alumina systems [3, 35-39], the questions above remain largely unanswered. The modern tools available to us, such as HAADF-STEM, in-situ FTIR, high-resolution XPS as well as catalytic measurements combined in this study allowed us to achieve a better understanding of the ceria/alumina system and its catalytic behaviour under industrially relevant high-temperature reactant exposure conditions [40-42].

We started exploring these catalysts by looking at commercially available Ceria on gamma-alumina samples with high surface area (Table S1) and various Ceria loadings: 8% and 50%. We also prepared our own ceria/alumina sample on the basis of platelet gamma-alumina with surface area 90 m^2/g, which was incipient-wetness impregnated with high-purity cerium nitrate and calcined at 800 ºC. The catalytic activity of these samples for NO reduction by CO in the presence of steam at representative GHSV ~ 150 L/g*hr is shown in Fig. 1. It can be inferred that all 3 samples have poor NO reduction activity. 50% Ceria sample had higher activity due to higher loadings of ceria (and atomically dispersed ceria initially present, see discussion in the text). Indeed, previously it was shown that ceria nanoparticles can catalyze NO reduction by CO (under dry conditions) as well as CO oxidation and water-gas-shift [27-31]. However, they demonstrate rather low activity in the absence of noble metals added to them. Electron microscopy images of the fresh samples reveal ceria nanoparticles mixed with alumina platelets (Fig. 2), as well as a rather sparse population of Ce single atoms (~ 1% by weight).
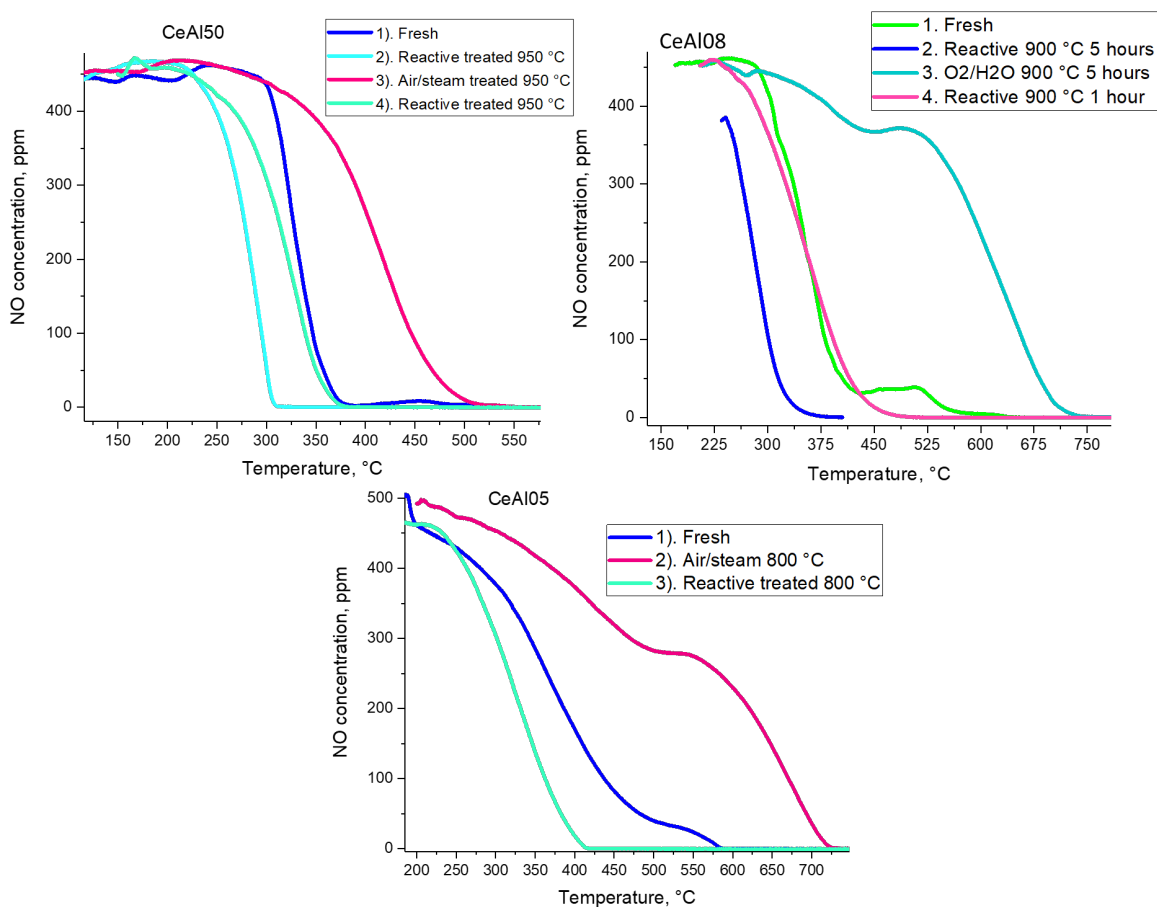
Figure 1. NO conversion for catalysts containing 8% ceria on alumina (CeAl08), 50% ceria on alumina (CeAl50) and 5% ceria of SBA-90 alumina (CeAl05). Sequential catalytic runs for the same catalyst are denoted as 1),2),3). Conditions: 120 mg catalyst. Total flow 300 ml/min. Concentrations: 460 ppm NO, 1750 ppm CO, ~2.6% H_2O, balanced with N_2. GHSV ~ 150 L/g*hr. Numbers 1)-4) denote activity measurements after each sequential treatment (treatments 1-4 performed in a sequence for each catalyst). Treatment time during each treatment (either air/steam or reactive/steam) is 5 hours, unless noted otherwise.

Later we will provide evidence that these sparse Ce+4 single atoms are associated with penta-Al sites and most likely poorly active for catalysis.

In gasoline vehicles, catalysts are typically exposed to harsh conditions in the flow of pollutants and steam and temperatures reaching 800-950 ºC [40-42]. It is generally believed that during this treatment, ceria sinters and catalytic activity diminishes. To test this possible effect, we exposed our Ce/Alumina samples to hydrothermal aging treatments of various severity (800-950 ºC). Afterwards, the samples were tested for NO reduction under the same typical conditions (Fig. 1). To our surprise, the activity not only did not decrease but instead we observed enhancement of NO reduction activity after this high temperature steam treatment. To understand whether this is just the effect of the temperature/steam or presence of reactants, we further treated the samples with air/steam at 900 and 950 ºC: under these treatments, we observed loss of activity, which is largely reversible: further reactive treatment restores the activity enhancement. Thus, treatment of the sample under reactive/steam vs air/steam conditions induces reversible changes to the sample, with the latter treatment being beneficial for catalysis. This unexpected result needed further investigation and so we turned to HAADF-STEM imaging of the samples exposed to reactive treatments vs. air/steam treatment Fig. 2. Dramatic changes are observed: for the 8 wt% Ce/Al₂O₃ sample

(CeAl08), reactive treatment induces essentially complete re-dispersion of ceria into isolated Ce atoms on the surface of alumina. Their density can be estimated by EDS analysis, and is ~ 7-8%. The sample further treated in air/steam, which is largely inactive, shows disappearance of single Ce atoms and their agglomeration into ceria nanoparticles. Similar trends are shown for CeAl50 sample after 950 ºC aging. The fresh sample contains significant density of single Ce atoms, possibly due to different synthesis conditions of this commercial sample: after reactive treatment enhancement is observed, but to a lower extent than for the 8%Ce/Alumina sample. However, air/steam treatment renders this sample poorly active consistent with disappearance of single Ce atoms and agglomeration of ceria into nanoparticles, as confirmed by HAADF-STEM. These findings indicate that high-temperature treatment (800-950 ºC) under reactive steam induces re-dispersion of ceria nanoparticles into isolated Ce atoms. These atoms are inferred to have much higher activity for NO reduction than supported ceria nanoparticles. They can be reversibly sintered in the flow of air/steam at high temperature into ceria nanoparticles. Now the following questions arise: 1). What

2
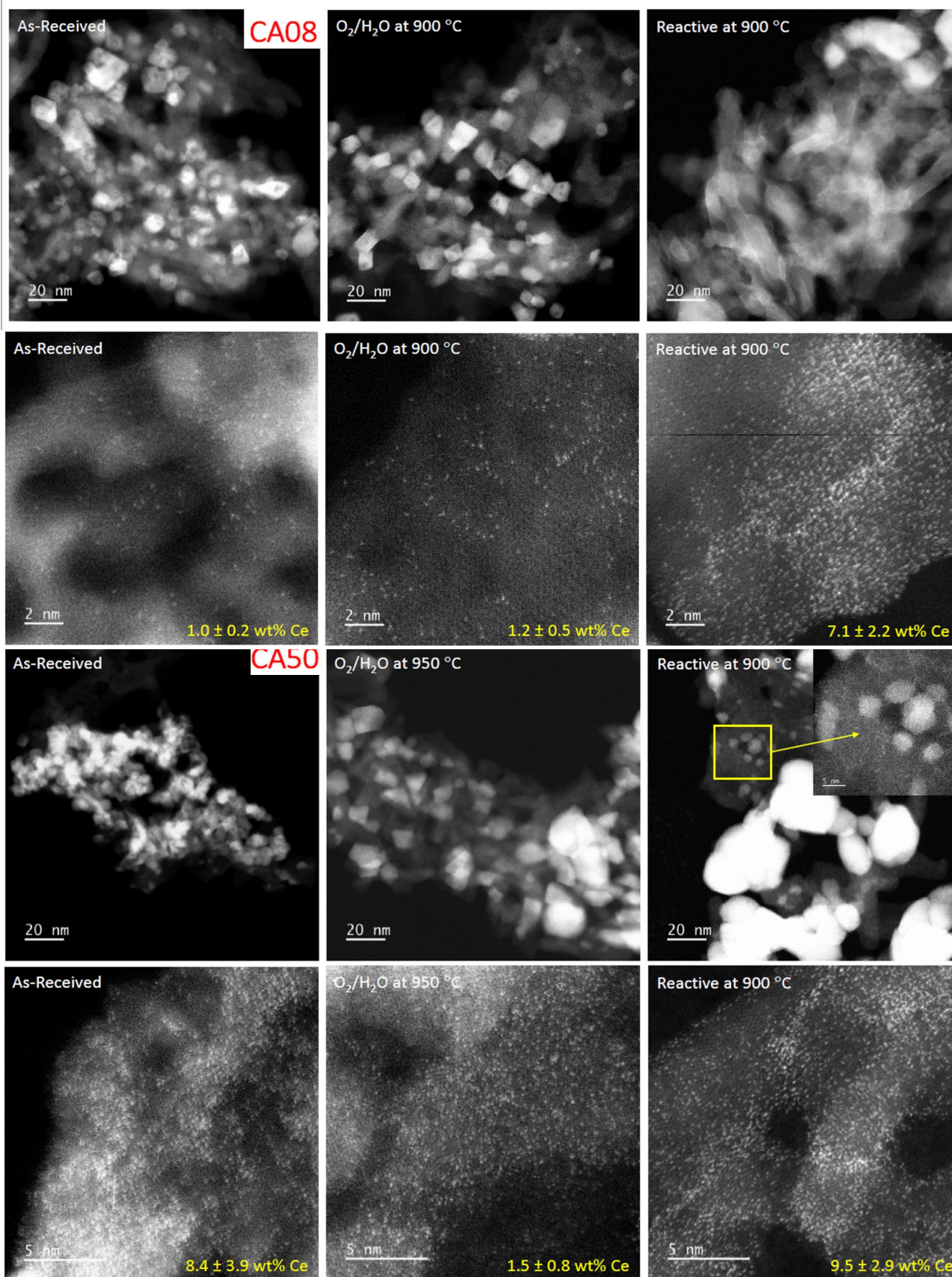
*Figure 2. HAADF-STEM images and corresponding EDS maps for 8 wt% Ce/g-Al$_2$O$_3$ sample (denoted as CA08) and 50% wt% Ce/g-Al$_2$O$_3$ sample (denoted as 50CeAl) in the fresh state, after reactive treatments (460 ppm NO, 1800 ppm CO, ~9-10 % H$_2$O balanced in nitrogen; GHSV ~150 L/g*hr) at 900-950 ºC, and further, after 900-950 ºC air/steam treatment (9-10% H$_2$O; GHSV ~ 150 L/g*hr).*

is the state of these ceria atoms? We suggest that they are likely +3 Ce atoms and prove it further with XPS. 2). How can they increase activity catalytic activity for NO reduction? This question is answered with the aid of infra-red measurements.

XPS was performed on the reactive-treated and air/steam treated samples (Fig. 3). It was observed that for air/steam treated samples the majority of Ce signal in 8CeAl resembles the typical signals for CeO$_2$ nanoparticles (Fig. 3) [52, 53]. XPS can estimate

XPS photoemission narrow scan spectral plot
Pure ceria-alumina 8Ce92Al samples

XPS photoemission narrow scan spectral plot
Pure ceria-alumina 50Ce50Al samples

Data file name	Area #	Sample description
071221.114.spe	HP7	8Ce92Al 900C reactive treatment
071221.110.spe	HP5	8Ce92Al 900C reactive treatment
071221.113.spe	HP6	8Ce92Al 900C O₂ H₂O
071221.109.spe	HP4	8Ce92Al 900C O₂ H₂O

Data file name	Area #	Sample description
071221.105.spe	HP5	CeAl NO CO H₂O 950C
070921.103.spe	HP2	CeAl NO CO H₂O 950C
071221.104.spe	HP3	CeAl O2 H₂O 950C
070921.102.spe	HP1	CeAl O2 H₂O 950C

Figure 3. Narrow XPS scans of the Ce3d region for CeAl08 and CeAl50 samples after reactive and air/steam treatments at 900 and 950 ºC. For each sample the scan was performed in 2 different locations of the sample to ensure reproducibility of the measurement and homogeneity of the sample.

concentration of Ce in the sample, with the value ~10.3 wt% (Table S2). Dramatic changes are observed for reactive treated samples in the presence of steam: most notably, significant fraction of Ce+3 species is now observed in the spectra (Fig. 3). We already know, on the basis of HAADF-STEM, that these are due to isolated Ce cations, and we can now conclude that their oxidation state is +3 [52]. Moreover, concentration of Ce in this sample increases to ~14.7%, fully consistent with CeO_2 nanoparticles re-dispersing and XPS depth profile can now "see" more available Ce, whereas in the case of ceria nanoparticles not all Ce within the CeO_2 nanoparticles can be accounted for. Similar changes are found for 50Ce50Al sample (Fig. 3, Tables S2,S3), fully consistent with reactivity data and HAADF-STEM images. In this case, however, due to a significantly higher amount of Ce present, even after alumina saturation capacity has been achieved with Ce, ceria nanoparticles still remain. Interestingly, subtle changes are also observed in the XPS spectra for Al2p and O1s signals (Figs. S1-S7). For the reactive treated sample, Al 2p signal is shifted by ~0.4 eV towards lower binding energies (73.8 vs. 74.2 eV), signifying subtle changes to the Al atoms on the surface induced by the presence of abundant Ce+3 ions. Preponderance of our data, thus, clearly suggests that high temperature reactive treatment induces formation of Ce+3

ions on the surface of alumina due to re-dispersion of ceria nanoparticles. These Ce+3 atoms provide catalytically active sites for NO reduction by CO. Furthermore, they also modify the surface of alumina. The most suitable technique to probe the surfaces is infra-red spectroscopy with probe molecules. We performed in-situ FTIR measurements with CeAl08 sample that has been reactive/steam pre-treatment at 900 ºC. CO adsorption at room temperature on thermally activated sample does not lead to any discernible CO signatures. This indicates that no penta Al sites are available on the surface since these are the only sites that can adsorb CO strongly under ambient conditions on alumina surfaces [43]. This result is further consistent with high-field solid-state 27Al NMR measurements (Fig. S8) showing absence of measurable penta Al in CeAl samples after various treatments.

We then performed CO adsorption at liquid nitrogen temperature (77 K; Fig. 4). It yields the intense C-O stretching band typical due to OH groups interacting with CO at 2173 cm⁻¹ and no discernible bands due to CO adsorption on bare penta or tetra-Al sites, implying lack thereof. Heating the sample in-situ in the presence of ~1 Torr oxygen at 800 ºC for 1 hour, followed by probing the surface with CO at 77 K provides further evidence of Ce migration on the surface and changes occurring to the Al surface: we observe the small but measurable shift of the C-O stretching band

4
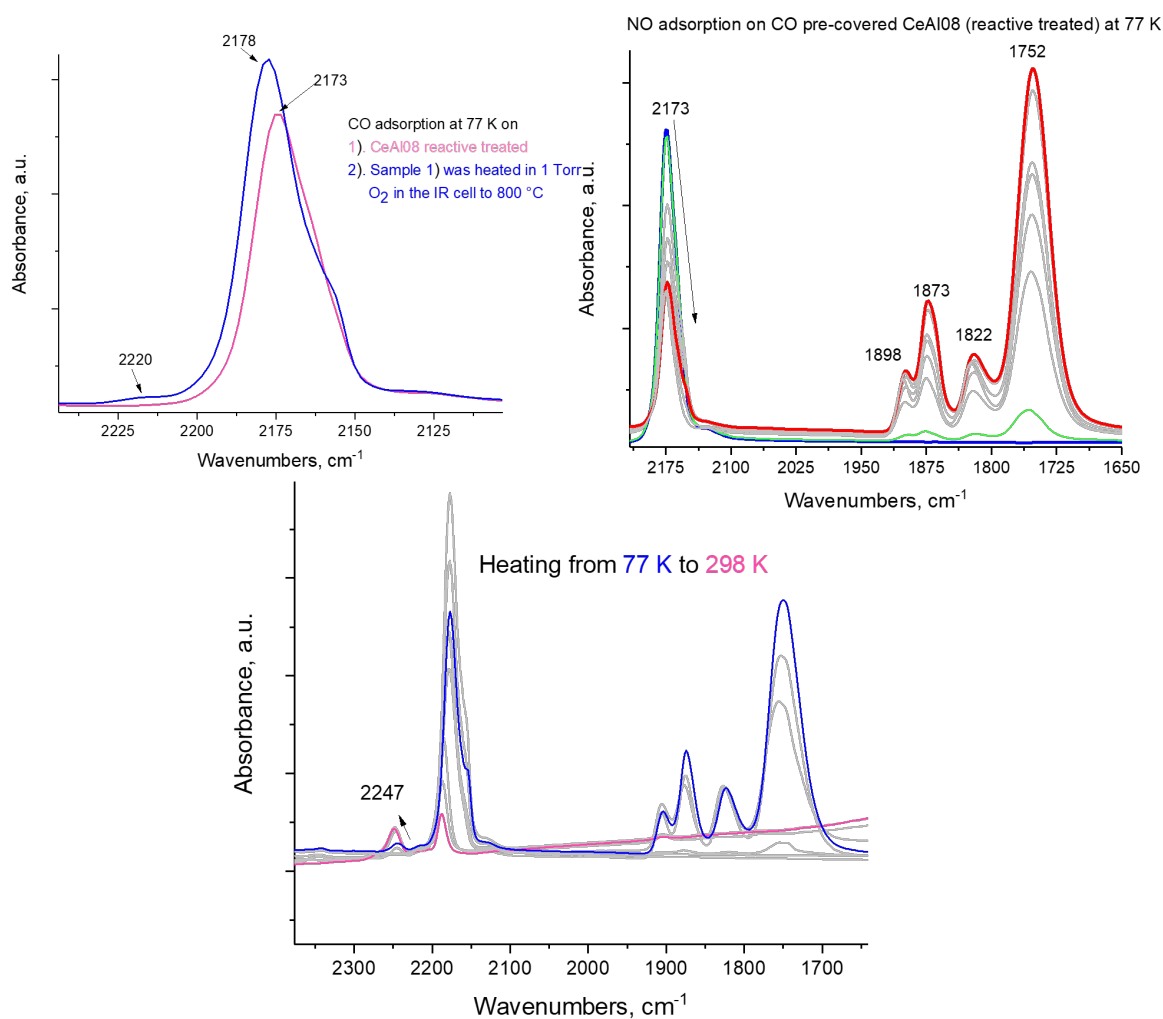
Figure 4. Infra-red measurements on CeAl08 (exposed to reactive treatment at 900 °C). A. Comparison of CO adsorption (2 Torr) on the sample „as is" (after reactive pre-treatment) and after exposure to 1 Torr O_2 in the infra-red cell at 77 K. B.NO (1 Torr) adsorption at 77 K on CO-preadsorbed CeAl08 samples. C. Heating from 77 to 298 K

of the Al-OH---CO complex from 2173 to 2178 cm^{-1} (Fig. 4). This is in excellent agreement with the XPS Al2p data that evidenced the subtle changes in the surface Al2p signal, showing on average slightly higher positive charge on Al in the oxidized sample with Ce+3 sites agglomerated into CeO_2 nanoparticles (and the corresponding Al-OH group). Furthermore, a new C-O stretching band appears ~2,220 cm^{-1}. We have previously shown that this band corresponds to CO directly adsorbed on tetra-Al sites [43]: indeed, Ce+3 dispersed on these sites prevent CO adsorption on them. Once they are removed by O_2 treatment, these sites become available for CO adsorption. Please note the lack of penta-Al sites on the sample after O_2 treatment with signatures ~ 2,235-2,240 cm^{-1}: this indicates that the penta Al sites are still occupied by the Ce cations and never become available for CO adsorption. It becomes clear that two types of atomically dispersed Ce sites are present on the surfaces of alumina: 1). Ce associated with penta-Al sites: this is consistent with HAADF-STEM images showing presence of a small amount (below 1.5 wt%) of Ce even after harsh O_2/H_2O treatments: it is well-known that these penta-sites adsorb metal cations strongly and they are present in similar amounts [44]. They remain on the surface during reactive/steam and air/steam treatment and are relatively

inactive. 2). Ce+3 cations that form upon redispersion of ceria nanoparticles during high temperature reactive-steam treatments in the presence of CO and NO: these Ce+3 cations are significantly more catalytically active than ceria nanoparticles, they reside on the surface and thus, they modify the surface of alumina. To highlight their activity, we performed in-situ co-adsorption NO/CO on reactive treated CeAl08 sample containing high density of atomically dispersed Ce+3 on alumina: first we adsorbed NO at 77 K on the CO saturated surface at 77 K, afterwards we heated the sample from 77 to 298 K (Fig. 4). Obviously, the presence of Ce allows us to observe bands below 2,000 cm^{-1} associated with NO adsorption. During this process, clear formation of N_2O is observed ~2,250 cm^{-1}[45]. Its formation is the direct evidence of Ce+3 participating in NO reduction. Although the exact mechanism of this process is not known at the moment, we propose the mechanism may involve two Ce(III) centers:

Ce(III) + 2 NO + Ce(III) → N_2O + Ce(IV)-O-Ce(IV)
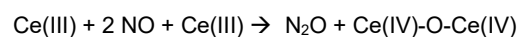
In order to restore the catalytic cycle, CO should reduce two resulting Ce(IV) centers:

5

$$Ce(IV)-O-Ce(IV) + CO \rightarrow CO_2 + Ce(III) + Ce(III)$$
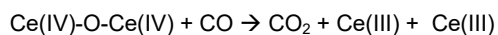
This reaction does not occur on ceria nanoparticles under these conditions. Only cerium centers in +3 oxidation state are highly reactive [54, 55].

should lead to deterioration of catalytic activity which is the opposite of what is observed for Rh on ceria-alumina (Fig. 5). The subsequent high-temperature treatment in air-steam leads to a decrease in NO reduction activity; now we can explain this phenomenon: agglomeration of cerium atoms into ceria nanoparticles occurs and Rh ions gets buried inside ceria
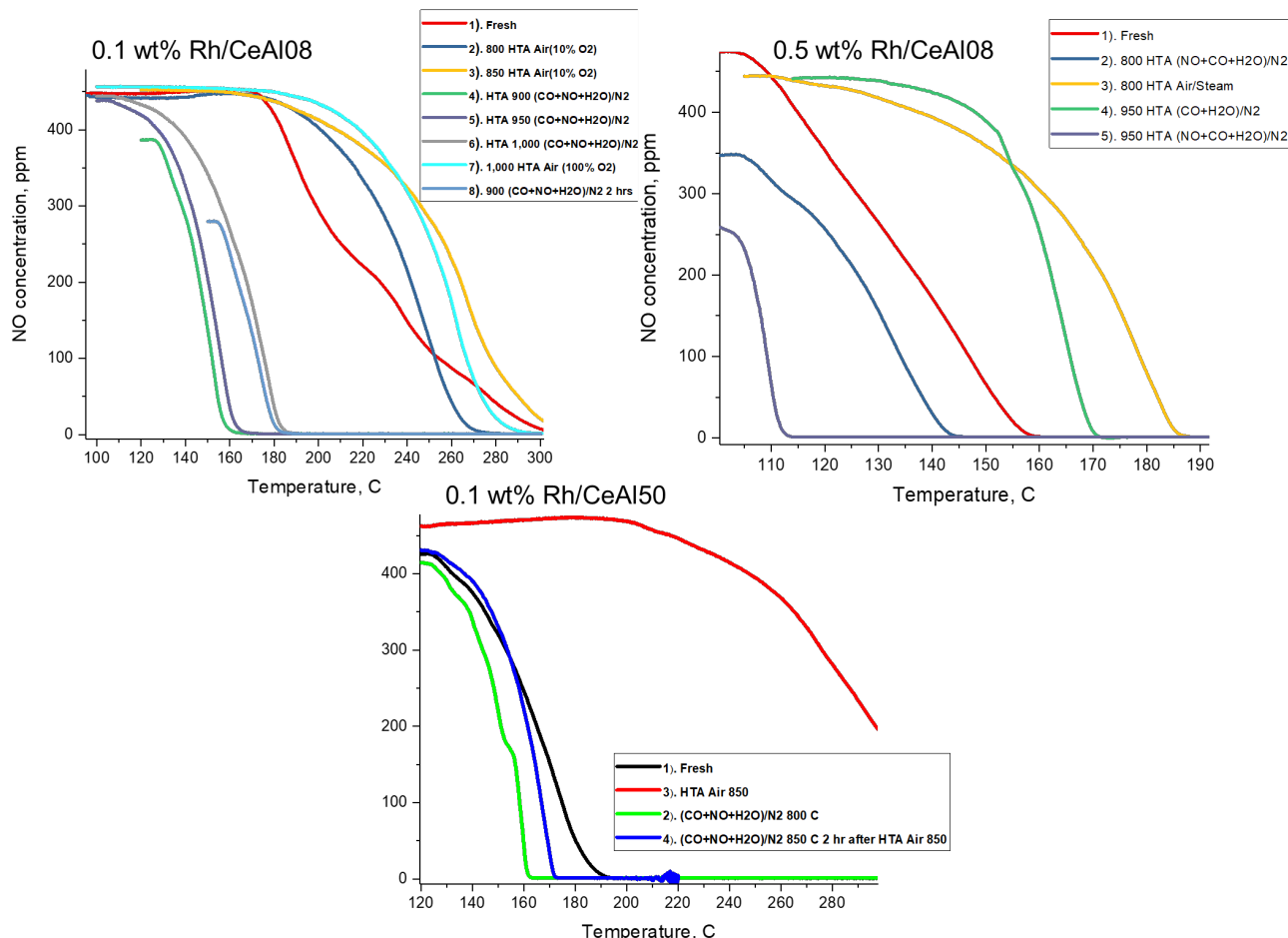
Figure 5. NO conversion for catalysts containing 0.1 wt% and 0.5 wt% Rh on CeAl08 and 0.1 wt% Rh on CeAl50. Sequential catalytic runs for the same catalyst are denoted as 1),2),3). Conditions: 120 mg catalyst. Total flow 300 ml/min. Concentrations: 460 ppm NO, 1750 ppm CO, ~2.6% H2O, balanced with N2. GHSV ~ 150 L/g*hr. Numbers 1)-4) denote activity measurements after each sequential treatment (treatments 1-4 performed in a sequence for each catalyst). Treatment time during each treatment (either air/steam or reactive/steam) is 5 hours, unless noted otherwise. HTA Air and HTA Air/steam are used interchangeably and signify hydrothermal aging in 10% O2/10%H2O. (CO+NO+H2O) treatment is reactive treatment in the presence of CO, NO and ~ 10% H2O.

We uncovered that reversible re-dispersion of ceria nanoparticles into Ce+3 ions on the surface of alumina under high temperature reactive treatment in the presence of steam dramatically increases NO reduction activity. Agglomeration of Ce+3 into ceria nanoparticles requires temperatures of ~800 ºC and above in the presence of air or air/steam. Our findings provide a broader picture of the behaviour of redox active oxides on alumina (potentially explaining behaviour of titania and other oxides) under real-world high temperature reactive treatments and provide an opportunity to further improve activity of the catalysts by supporting noble metals on the catalysts with maximized number of Ce+3 ions [45-51]. To demonstrate the extension of this approach, we loaded the CeAl08 and CeAl50 samples with 0.1 and 0.5 wt% Rh: loading Rh on ceria/alumina [45] results in dramatic promotion of the catalyst activity after high-temperature reactive treatment. It is commonly believed that such treatment

nanoparticles, becoming unavailable for adsorption and reaction. Redispersion of Ce during reactive treatment at high temperatures exposes all (or majority of) catalytically active Rh and Ce+3 back to reactants restoring catalytic activity.

Acknowledgements

*Corresponding authors.

Conflict of interest

No conflicts to éclair.

(1) J. C. Summers and S. A. Ausen, J. Catal., 58, 131 (1979).
(2) G. Kim, Ind. Eng. Chem. Prod. Res. Dev., 21, 267 (1982).
(3) H. S. Gandhi, A. G. Piken, M. Shelef, R. G. Delosh, SAE Paper 760201, 55 (1976).
(4) A. A. Bhattacharyya, G. M. Woltermann, J. S. Yoo, J. A. Karch, W. E. Cormier, Ind. Eng. Chem. Res., 27, 1356 (1988).
(5) Trovarelli, A. Catal. Rev.: Sci. Eng. 1996, 38, 439−520.
(6) McCabe, R. W.; Trovarelli, A. Appl. Catal., B 2016, 197, 1.
(7) Vivier, L.; Duprez, D. ChemSusChem 2010, 3, 654−678.
(8) Montini, T.; Melchionna, M.; Monai, M.; Fornasiero, P. Chem.
(9) Rev. 2016, 116, 5987−6041.
(10) Gorte, R. J. AIChE J. 2010, 56, 1126−1135.
(11) Trovarelli, A.; Fornasiero, P. In Catalysis by Ceria and Related Materials, 2nd ed.; Imperial College Press: London, 2013.
(12) Carretin, S.; Concepcion, P.; Corma, A.; Nieto, J. M. L.; Puntes, V. F. Angew. Chem., Int. Ed. 2004, 43, 2538−2540.
(13) Divins, N. J.; Angurell, I.; Escudero, C.; Perez-Dieste, V.; Llorca, J. Science 2014, 346, 620−623.
(14) Cargnello, M.; Doan-Nguyen, V. V. T.; Gordon, T. R.; Diaz, R. E.; Stach, E. A.; Gorte, R. J.; Fornasiero, P.; Murray, C. B. Science 2013, 341, 771−773.
(15) Rodriguez, J. A.; Grinter, D. C.; Liu, Z.; Palomino, R. M.; Senanayake, S. D. Chem. Soc. Rev. 2017, 46, 1824−1841.
(16) Farmer, J. A.; Campbell, C. T. Science 2010, 329, 933−936.
(17) Dvorak, F.; Farnesi Camellone, M.; Tovt, A.; Tran, N. D.; Negreiros, F. R.; Vorokhta, M.; Skala, T.; Matolinova, I.; Myslivecek, J.; Matolin, V.; Fabris, S. Nat. Commun. 2016, 7, 10801.
(18) Jones, J.; Xiong, H. F.; Delariva, A. T.; Peterson, E. J.; Pham, H.; Challa, S. R.; Qi, G. S.; Oh, S.; Wiebenga, M. H.; Hernandez, X. I. P.; Wang, Y.; Datye, A. K. Science 2016, 353, 150−154.
(19) Vayssilov, G. N.; Lykhach, Y.; Migani, A.; Staudt, T.; Petrova, G. P.; Tsud, N.; Skala, T.; Bruix, A.; Illas, F.; Prince, K. C.; Matolin, V.; Neyman, K. M.; Libuda, J. Nat. Mater. 2011, 10, 310−315.
(20) Mudiyanselage, K.; Senanayake, S. D.; Feria, L.; Kundu, S.; Baber, A. E.; Graciani, J.; Vidal, A. B.; Agnoli, S.; Evans, J.; Chang, R.; Axnanda, S.; Liu, Z.; Sanz, J. F.; Liu, P.; Rodriguez, J. A.; Stacchiola, D. J. Angew. Chem., Int. Ed. 2013, 52, 5101−5105.
(21) Xiaoding X, Moulijn JA (1996) Energy Fuels 10:305
(22) Wang W, Wang S, Ma X, Gong J (2011) Chem Soc Rev 40:3703
(23) Towler G, Lynn S (1994) Chem Eng Sci 49:2585
(24) Park SE, Han SC (2004) J Ind Eng Chem 10:1257
(25) Ansary MB, Park SE (2012) Energy Environ Sci 5:9419
(26) Newsome DS (1980) Catal Rev 21:275
(27) M. Daturi, N. Bion, J. Saussey, J.C. Lavalley, C. Hedouin, T. Seguelong, G. Blanchard, Physical Chemistry Chemical Physics 3 (2001) 252-255.
(28) Tana, Zhang M, Li J, Li H, Shen W (2009) Catal Today 148:179
(29) Zhou K, Wang X, Sun X, Peng Q, Li Y (2005) J Catal 229:206
(30) Liu X, Zhou K, Wang L, Wang B, Li Y (2009) J Am Chem Soc 131:3140
(31) Liu L, Cao Y, Sun W, Yao Z, Liu B, Gao F, Dong L (2011) Catal Today 175:48
(32) Pereira-Hernandez, X. I.; DelaRiva, A.; Kunwar, D.; Xiong, H.; Sudduth, B.; Engelhard, M.; Kovarik, L.; Murayev, V.; Hensen, E.; Wang, Y.; Datye, A. K. Nat. Commun. 2019, DOI: 10.1038/s41467-019-09308-5
(33) Datye, A.; Wang, Y. Natl. Sci. Rev. 2018, 5, 630−632.
(34) Nie, L.; Mei, D.; Xiong, H.; Peng, B.; Ren, Z.; Hernandez, X. I. P.; DeLaRiva, A.; Wang, M.; Engelhard, M. H.; Kovarik, L.; Datye, A. K.; Wang, Y., Science 2017, 358, 1419.
(35) Twigg, M.V., Haren Gandhi 1941-2010: Contributions to the Development and Implementation of Catalytic Emissions Control Systems. Platinum Metals Review, 2011. 55(1): p. 43-53.
(36) J.Z. Shyu, W.H. Weber, H.S. Gandhi, J. Phys. Chem., 92 (1988), pp. 4964-4970
(37) J. Z. Shyu, K. Otto, W. L. H. Watkins, G. W. Graham, R. K. Belitz, H. S. Gandhi, J. Catal 1988, 114, 23-33.
(38) I. Z. Koleva, H. A. Aleksandrov, G. N. Vayssilov, R. Duarte, J. A. van Bokhoven, Phys. Chem. Chem. Phys., 2015,17, 22389-22401
(39) G. Kim, Ind. Eng. Chem. Prod. Res. Dev. 1982, 21, 2, 267–274
(40) Rappé, K.G., et al., Emission Control Science and Technology, 2019. 5(2): p. 183-214.
(41) K. Khivantsev, J.-H. Kwak, N. R. Jaegers, Y. Wang, J. Szanyi, L. Kovarik, Chemrxiv 2021 doi:10.33774/chemrxiv-2021-tq1kw
(42) H Jeong, O Kwon, BS Kim, J Bae, S Shin, HE Kim, J Kim, H Lee, Nature Catalysis 3 (4), 368-375 (2020)
(43) K. Khivantsev, N. R. Jaegers, J.-H. Kwak, J Szanyi, L Kovarik, Angewandte Chemie International Edition 2021, 133 (32), 17663-17671
(44) J. H. Kwak, J. Hu, D. Mei, C.-W. Yi, D. H. Kim, C. H. F. Peden, L. F. Allard, J. Szanyi, Science 2009, 325, 1670– 1673.
(45) Khivantsev, K.; Vargas, C. G.; Tian, J.; Kovarik, L.; Jaegers, N. R.; Szanyi, J.; Wang, Y. Angew. Chem., Int. Ed. 2021, 60, 391−398
(46) Datye, A.; G. Hua, Nature Communications, 2021. 12(1): p. 1-3.
(47) Xiong, H., A.K. Datye, Y. Wang, Advanced Materials, 2021: p. 2004319.
(48) P. Bourges, S. Lunati, G. Mabilon, Catalysis And Automotive Pollution Control IV 116, 213 (1998)
(49) J. R. Theis, A. Getsoian, C. Lambert, SAE International Journal of Fuels and Lubricants 2017 10 (2), 583-592
(50) A. B. Getsoian, J. R. Theis, W. A. Paxton, M. J. Lance, C. K. Lambert, Nature Catalysis 2019 2 (7), 614-622
(51) Future Automotive Aftertreatment Solutions: The 150°C Challenge Workshop Report. 2013.
(52) M. A. Henderson, C. L. Perkins, M. Engelhard, S. Thevuthasan, C. H. F. Peden, Surface Science 2003 526 (1), 1-18.
(53) S. Kuchibhatla, A. S. Karakoti, D. R. Baer, S. Samudrala, M. Engelhard, J. Amonette, S. Thevuthasan, S. Seal, The Journal of Physical Chemistry C 2012 116 (26), 14108-14114
(54) M. Y. Mihaylov, E. Z. Ivanova, H. A. Aleksandrov, P. S. Petkov, G. N. Vayssilov, K. I. Hadjiivanov, Applied Catalysis B: Environmental 2015 176, 107-119
(55) M. Y. Mihaylov, E. Z. Ivanova, G. N. Vayssilov, K. I. Hadjiivanov, Catalysis Today 2020, 357, 613-620

Dramatic enhancement of NO reduction activity via reversible re-dispersion of CeO$_2$ nanoparticles into Ce^{+3} atoms on alumina under high temperature reactive treatment

Konstantin Khivantsev,[a]*† Hien Pham[b]†, Mark H. Engelhard[a]†, Xiahong Shari Li[a], Jinshu Tian[a], Yipeng Sun[d], Pascaline Tran[d], Trent R. Graham[a], Dong Jiang[c], János Szanyi[a], Abhaya Datye[c]* and Yong Wang[a,c]*

Supplementary Information

Materials and Methods

Cerium nitrate hexahydrate was purchased from Sigma with purity of 99.999%. Commerically available SBA-90 gamma-alumina with surface area 90 m^2/g was used for the synthesis of 5 wt% Ceria/Alumina sample. Commercial samples with nominal 8% and 50% ceria supported on gamma-alumina were supplied by BASF.

To prepare the loadings of Rh on ceria of 0.1 and 0.5 wt%, the desired amount of Rh precursor (rhodium nitrate hydrate, Sigma) was dissolved in the minimum amount of water (total volume approximately equivalent to the pore of volume ceria) and added with a micropipette to the desired amount of sample while continuously stirring with the spatula to ensure uniformity. The obtained wetted powder was dried under N$_2$ flow at 80 ^{o}C, and then calcined at 600 ^{o}C for 1 hour in a regular muffle furnace with a ramp rate of 5 ^{o}C/min. The as-prepared Rh/Ceria-alumina catalysts were pressed, crushed and sieved to 60-80 mesh, and subsequently used as catalysts.

Hydrothermal aging with oxygen (HTA) was performed at the desired temperature for 5 hours *unless noted otherwise in the text) in a flow reactor with GHSV ~ 150 L/g*hr. The gas mix, used for HTA, containing air and 10% H$_2$O and ~10% oxygen. Reactive treatment (hydrothermal aging) was performed at the desired temperature in the presence of CO, NO, nitrogen and 10% H$_2$O with GHSV ~ 150 L/g*hr for 5 hours (unless noted otherwise in the text).

(NO+CO) catalytic experiments were conducted in a plug-flow reactor system with powder samples (120 mg, 60–80 mesh) loaded in a quartz tube, using a synthetic gas mixture containing 460 ppm of NO and 1,750 ppm CO balanced with N$_2$ at a flow rate of 310 sccm (corresponding to GHSV 150 L/g*hr) in the presence of 2.6 % water vapor. All the gas lines were heated to over 100 °C. Concentrations of reactants and products were measured by an online MKS MultiGas 2030 FTIR gas analyzer with a gas cell maintained at 191 °C. Two four-way valves were used for gas switching between the reactor and the bypass. Heating and cooling rates were 4 K/min.

BET surface areas were conducted on a Micromeritics ASAP-2000 instrument with Ar as the adsorbate. Prior to analysis, the samples were dehydrated under vacuum for 3 hours at 250 °C.

Samples were dispersed in ethanol and mounted on holey carbon grids for examination in a JEOL NeoARM 200CF transmission electron microscope (TEM) equipped with spherical aberration correction to allow atomic resolution imaging, and an Oxford Aztec Energy Dispersive System (EDS) for elemental analysis. The microscope is equipped with two large area JEOL EDS detectors for higher throughput in acquisition of x-ray fluorescence signals. Images were recorded in annular dark field (ADF) mode and in annular bright field (ABF) mode.

X-ray Photoelectron Spectroscopy (XPS) experiments were performed using a Physical Electronics Quantera scanning X-ray microprobe. This system uses a focused monochromatic Al Kα X-ray (1486.7 eV) source for excitation and a spherical section analyzer. The instrument has a 32 element multichannel detection system. The 80 W X-ray beam focused to 100 μm diameter was rastered over a 1.1 × 0.1 mm rectangle on the sample. The X-ray beam was incident normal to the sample and the photoelectron detector was at 45° off-normal. High-energy-resolution spectra were collected using a pass-energy of 69.0 eV with a step size of 0.125 eV. Note that the samples experienced variable degrees of charging. Low-energy electrons at ~1 eV, 20 μA and low-energy Ar+ ions were used to minimize this charging.

^{27}Al MAS NMR spectroscopy was performed using a 14.1 T Bruker NMR. At this field strength, the corresponding ^{27}Al Larmor frequency is 156.375 MHz. Spectra were acquired using a MASDVT600W2 BL2.5 X/Y/H probe at a temperature of room temperature. Spectra were acquired following a single direct excitation pulse, with a total collection of 512 transients and an acquisition time of 9.9 ms. A delay between transients of 0.5 s was used, and the excitation pulse was a single, π/20 liquid-state pulse of 0.450-μs duration. The liquid-state pulse widths are referenced by nutation experiments performed on a 1 M $Al(H_2O)_6^{3+}$ solution, which was prepared via dissolution of aluminum chloride hexahydrate ($AlCl_3 \cdot 6H_2O$, ≥99%, Sigma-Aldrich) in H_2O. The chemical shifts of the ^{27}Al MAS NMR spectra are also referenced to this 1 M $Al(H_2O)_6^{3+}$ solution, for which the resonance of the reference solution was assigned to 0 ppm. The ^{27}Al MAS NMR spectra were collected at a MAS spin rate of 20 kHz. The MAS NMR spectra were then processed in Mestrenova (version 14.01–23,559, released 2019-06-07, Mestrelab Research S.L.), where the free induction decay was zero filled once to 18.8 ms and then 5 Hz of exponential line broadening was applied.

The *in-situ* transmission IR experiments were conducted in a home-built cell housed in the sample compartment of a Bruker Vertex 80 spectrometer, equipped with an MCT detector and operated at 4 cm^{-1} resolution. The powder sample was pressed onto a tungsten mesh which, in turn, was mounted onto a copper heating assembly attached to a ceramic feedthrough. The

sample could be resistively heated, and the sample temperature was monitored by a thermocouple spot welded onto the top center of the W grid. The cold finger on the glass bulb containing CO was cooled with liquid nitrogen to eliminate any contamination originating from metal carbonyls, while NO was cleaned with multiple freeze–pump–thaw cycles. Prior to spectrum collection, a background with the sample in the IR beam was collected. Each spectrum reported is obtained by averaging 64 scans.

High Energy Resolution Photoemission Spectra of the Ce 3d Region
CeO_2 reference for comparison
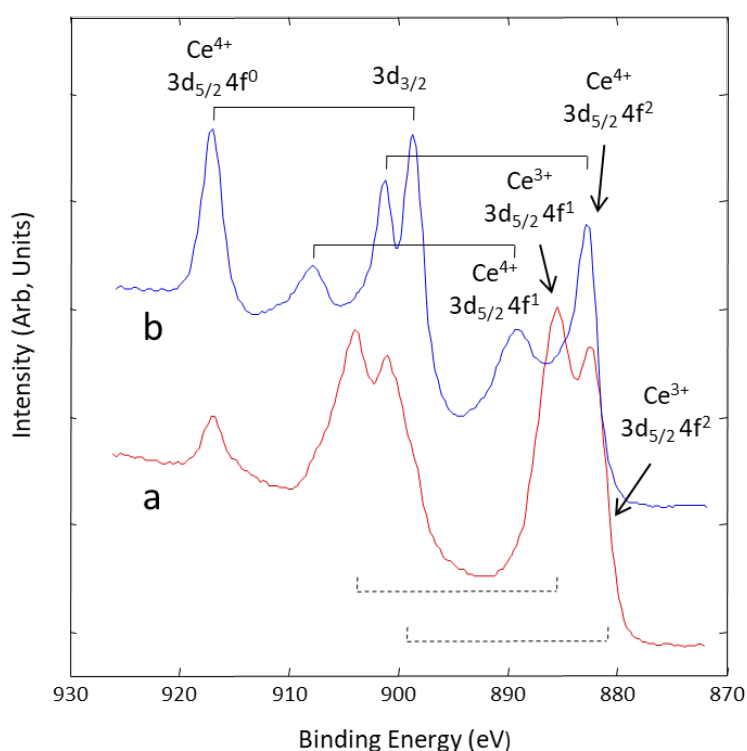
a = Mostly Ce^{3+} with some Ce^{4+}

b = Mostly Ce^{4+}

The brackets show spin orbit pairs (5/2 and 3/2) for Ce^{4+} (solid lines) and Ce^{3+} (dashed lines)

Figure S1. Reference Ce 3d XPS spectra for ceria nanoparticles containing mostly Ce+4 (sample b). And reference for Ce+3 sample (sample a; reduced in-situ with H₂), containing a significant fraction of Ce+3.

XPS photoemission narrow scan spectral plot
Pure ceria-alumina CeAl08
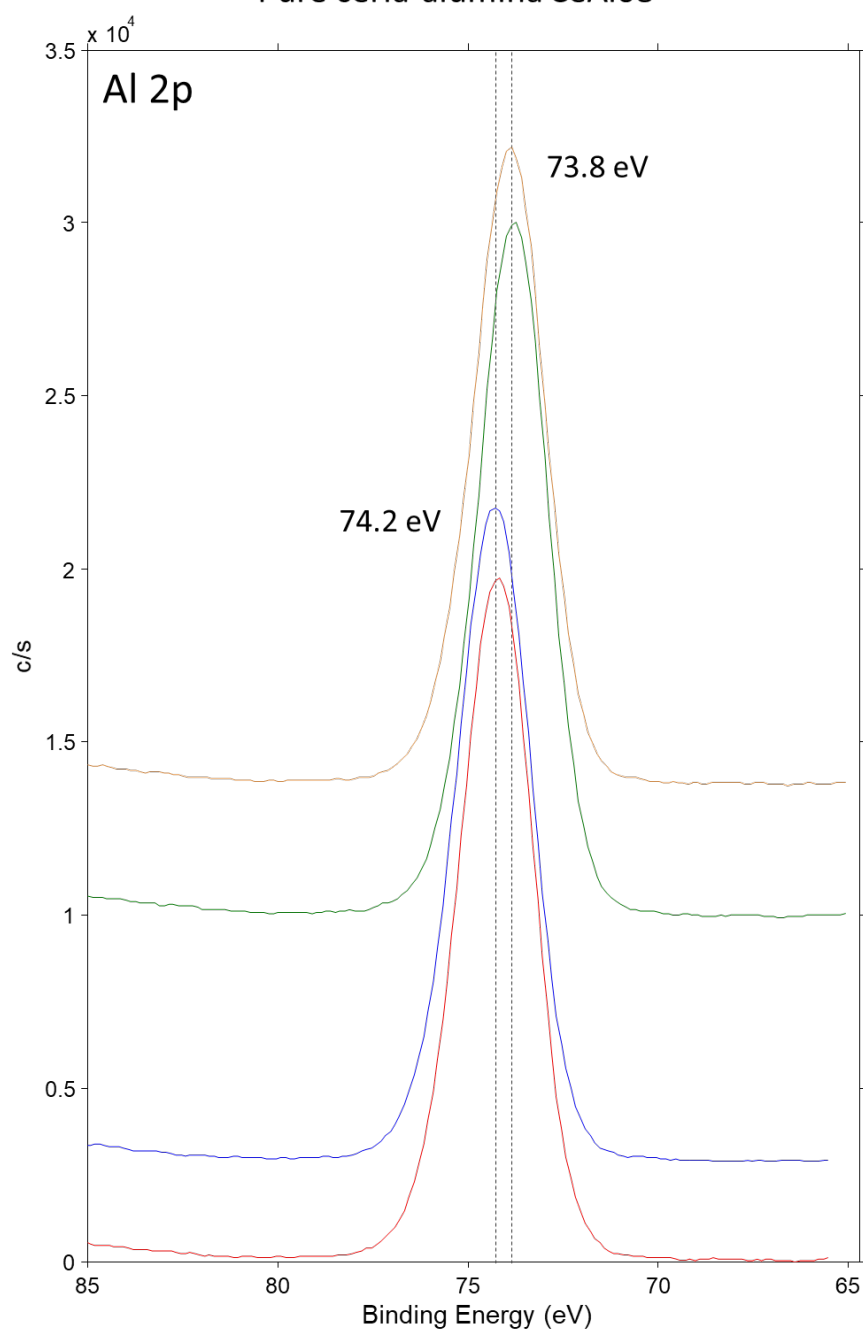
Data file name	Area #	Sample description
071221.114.spe	HP7	8Ce92Al 900C reactive
071221.110.spe	HP5	8Ce92Al 900C reactive
071221.113.spe	HP6	8Ce92Al 900C O_2 H_2O
071221.109.spe	HP4	8Ce92Al 900C O_2 H_2O

Figure S2. *Narrow XPS scans of the Al2p region for CeAl08 samples after reactive and air/steam treatments at 900 ºC. For each sample the scan was performed in 2 different locations of the sample to ensure reproducibility of the measurement and homogeneity of the sample.*

XPS photoemission narrow scan spectral plot
Pure ceria-alumina CeAl08
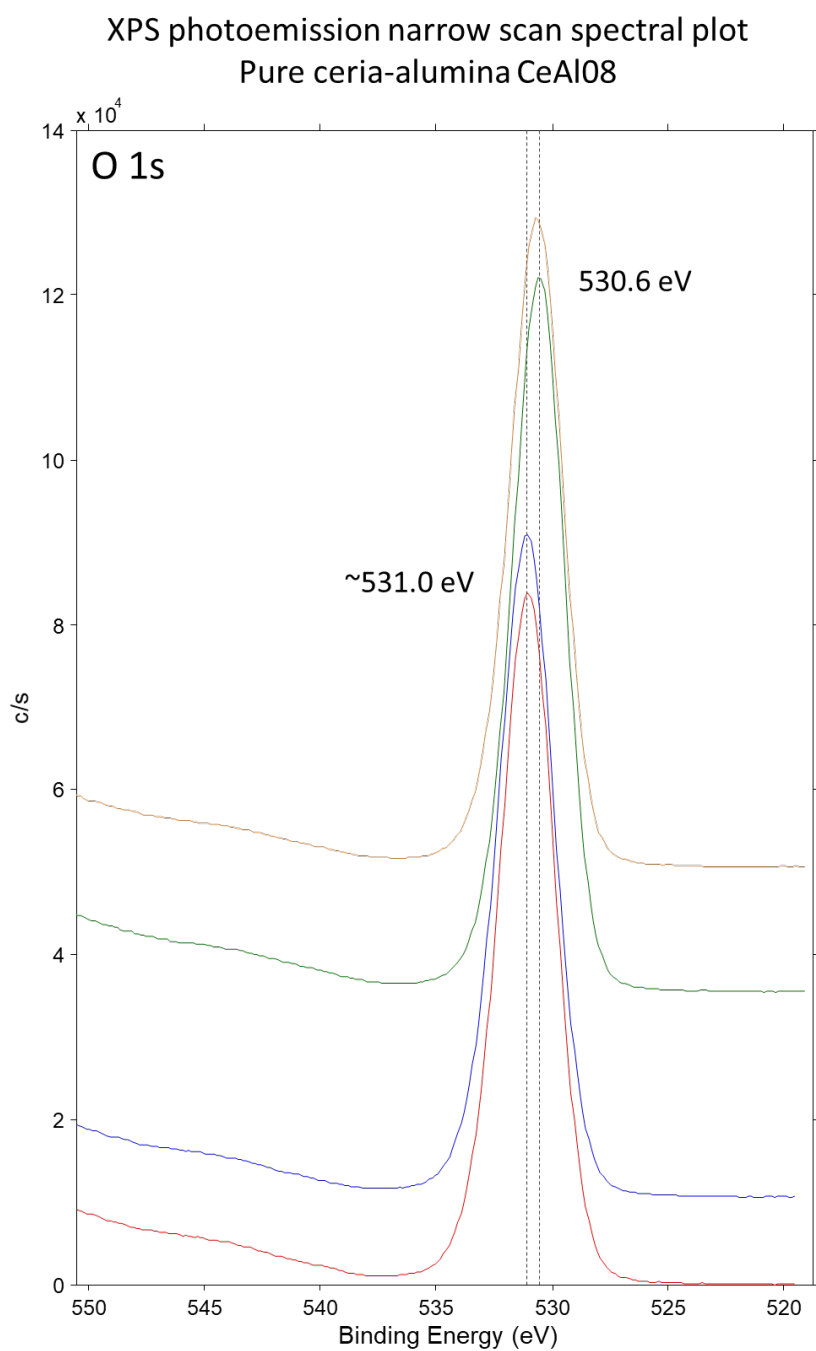
Data file name	Area #	Sample description
071221.114.spe	HP7	8Ce92Al 900C reactive
071221.110.spe	HP5	8Ce92Al 900C reactive
071221.113.spe	HP6	8Ce92Al 900C O_2 H_2O
071221.109.spe	HP4	8Ce92Al 900C O_2 H_2O

Figure S3. Narrow XPS scans of the O1p region for CeAl08 samples after reactive and air/steam treatments at 900 ºC. For each sample the scan was performed in 2 different locations of the sample to ensure reproducibility of the measurement and homogeneity of the sample.

XPS photoemission narrow scan spectral plot
Pure ceria-alumina CeAl08
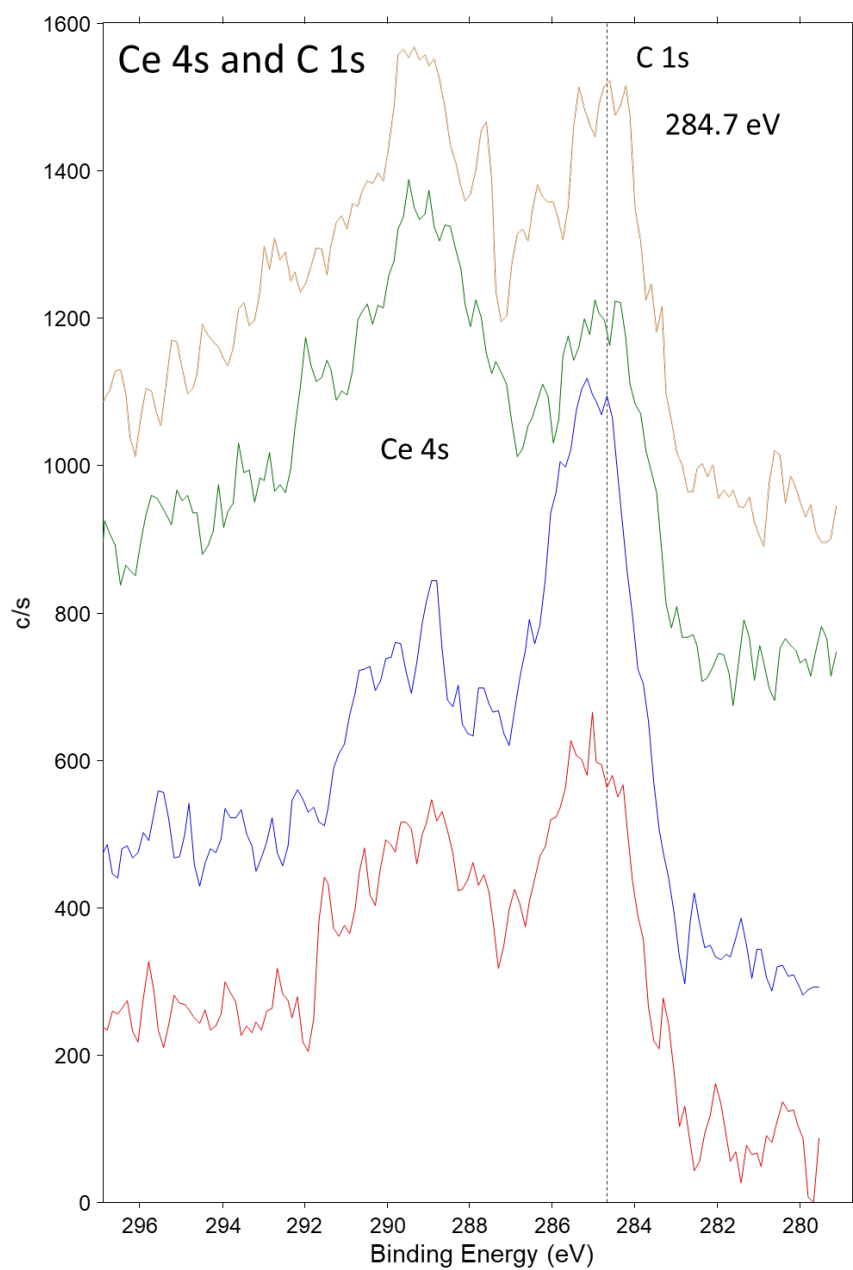
Data file name	Area #	Sample description
071221.114.spe	HP7	8Ce92Al 900C reactive
071221.110.spe	HP5	8Ce92Al 900C reactive
071221.113.spe	HP6	8Ce92Al 900C O_2 H_2O
071221.109.spe	HP4	8Ce92Al 900C O_2 H_2O

Figure S4. Narrow XPS scans of the C1s and Ce4s regions for CeAl08 samples after reactive and air/steam treatments at 900 ºC. For each sample the scan was performed in 2 different locations of the sample to ensure reproducibility of the measurement and homogeneity of the sample.
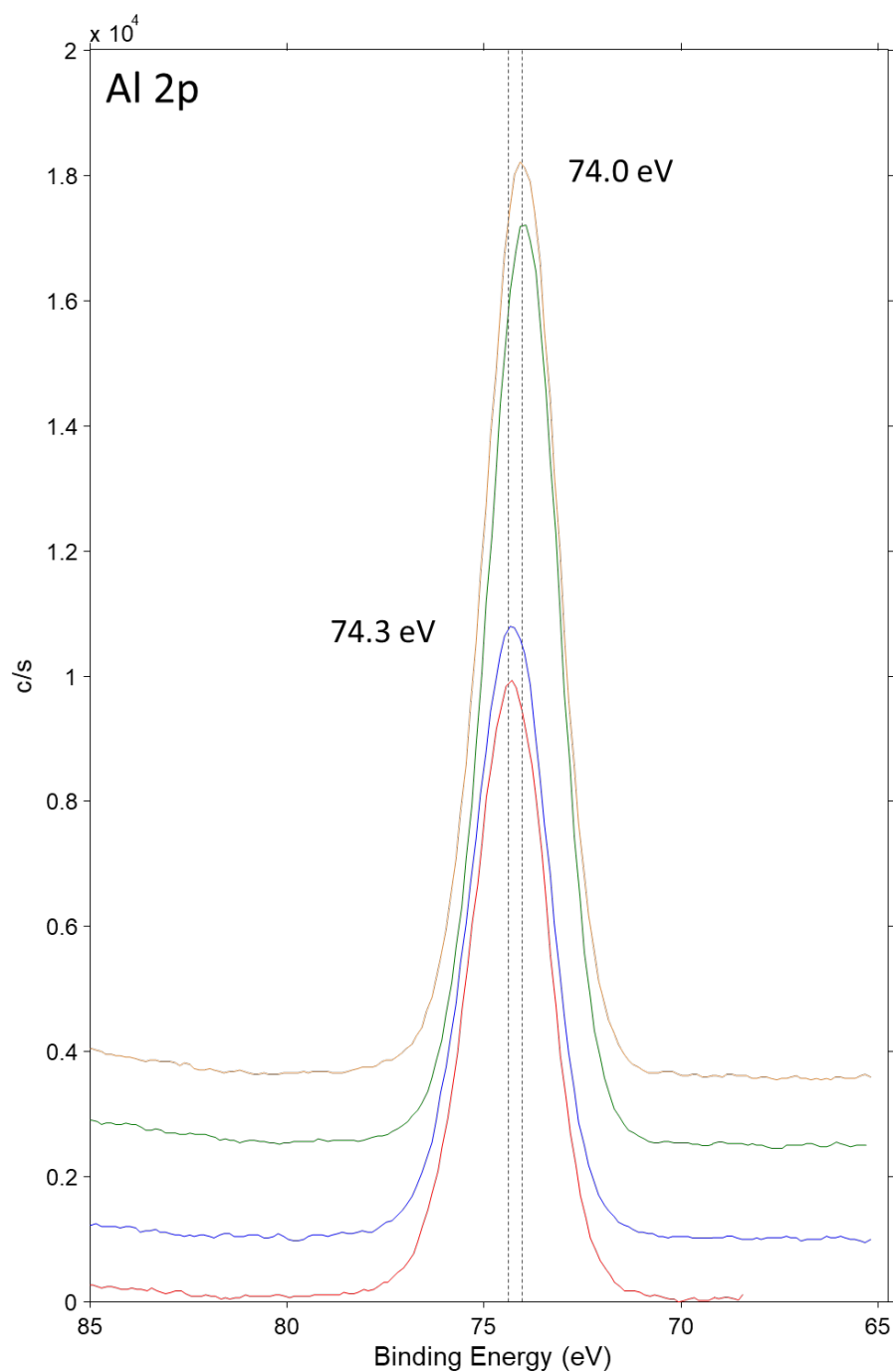
Figure S5. Narrow XPS scans of the Al2p region for CeAl50 samples after reactive and air/steam treatments at 950 ºC. For each sample the scan was performed in 2 different locations of the sample to ensure reproducibility of the measurement and homogeneity of the sample.

XPS photoemission narrow scan spectral plot
Pure ceria-alumina CeAl50

O 1s

530.8 eV

~531.7 eV
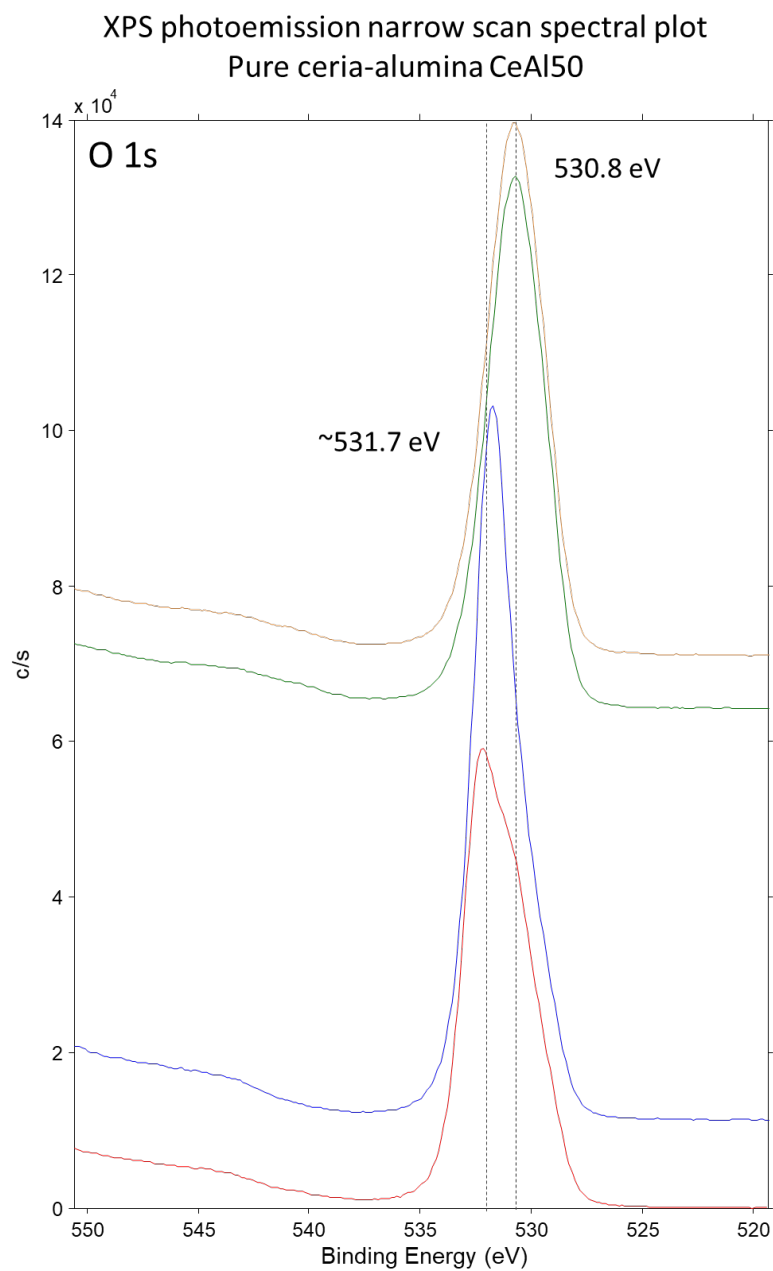
Data file name	Area #	Sample description
071221.105.spe	HP5	CeAl NO CO H_2O 950C
070921.103.spe	HP2	CeAl NO CO H_2O 950C
071221.104.spe	HP3	CeAl O2 H_2O 950C
070921.102.spe	HP1	CeAl O2 H_2O 950C

Figure S6. Narrow XPS scans of the O1p region for CeAl50 samples after reactive and air/steam treatments at 950 ⁰C. For each sample the scan was performed in 2 different locations of the sample to ensure reproducibility of the measurement and homogeneity of the sample.

XPS photoemission narrow scan spectral plot
Pure ceria-alumina CeAl50
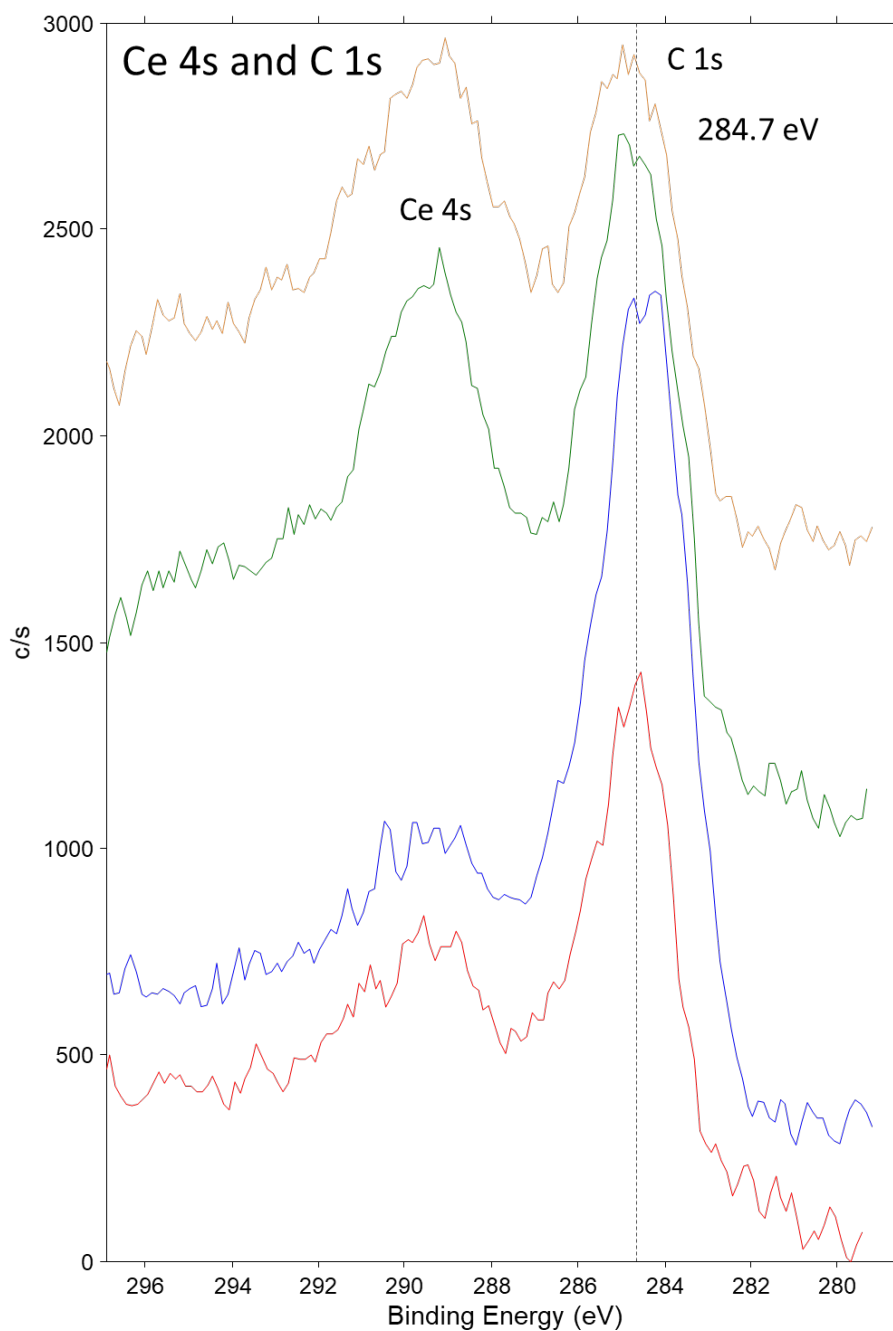
Data file name	Area #	Sample description
071221.105.spe	HP5	CeAl NO CO H_2O 950C
070921.103.spe	HP2	CeAl NO CO H_2O 950C
071221.104.spe	HP3	CeAl O2 H_2O 950C
070921.102.spe	HP1	CeAl O2 H_2O 950C

Figure S7. Narrow XPS scans of the C1s and Ce4s regions for CeAl50 samples after reactive and air/steam treatments at 950 ºC. For each sample the scan was performed in 2 different locations of the sample to ensure reproducibility of the measurement and homogeneity of the sample.
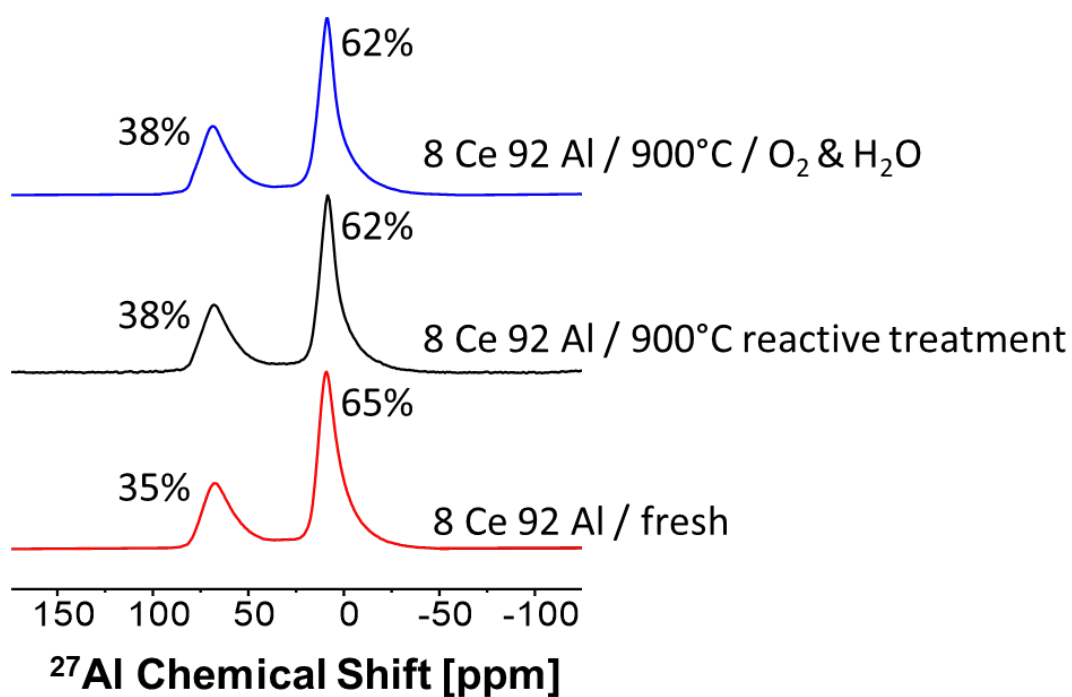
Figure S8. Single pulse, direct excitation ^{27}Al MAS NMR at 14.1 T with a MAS rate of 32 kHz. The integral of tetrahedral (70 ppm) and octahedral Al (10 ppm) are annotated.

Table S1. BET Surface areas of various synthesized samples.

Sample	BET area, m²/g
CeAl08	141
CeAl08 Reactive/900 °C	109
CeAl08 Air/steam/900 °C	90
CeAl50	169
CeAl50 Reactive/950 °C	
CeAl50 Air/steam/950 °C	70
CeAl05	90
Ce/Al05 (SBA-90 alumina) Reactive/800 °C	94
Ce/Al05 (SBA-90 alumina) Air/Steam/800 °C	95

Table S2

Weight concentrations of individual elements estimated from XPS data for CeAl08

```
-------------------------
   Weight % Table
-------------------------
File Name        Area Name  Area Comment                          C1s      O1s      Al2p     Ce3d

071221.109.spe   HP4        8Ce92Al 900C O2 H2O                   0.30     44.46    44.80    10.44
071221.113.spe   HP6        8Ce92Al 900C O2 H2O                   0.45     44.18    45.09    10.28
071221.110.spe   HP5        8Ce92Al 900C reactive treatment       0.25     42.17    42.95    14.63
071221.114.spe   HP7        8Ce92Al 900C reactive treatment       0.26     41.90    43.13    14.71
```

Table S3

Weight concentrations of individual elements estimated from XPS data for CeAl50

```
-------------------------
   Weight % Table
-------------------------
File Name        Area Name  Area Comment              C1s    O1s     Al2p    Ce3d

070921.102.spe   HP1        CeAl50 O2 H2O 950C        0.95   48.88   30.59   19.59
071221.104.spe   HP3        CeAl50 O2 H2O 950C        1.63   53.86   27.59   16.92
070921.103.spe   HP2        CeAl50 NO CO H2O 950C     1.00   39.59   33.03   26.38
071221.105.spe   HP5        CeAl50 NO CO H2O 950C     0.70   38.99   33.04   27.26
```